Journal of Molecular Graphics and Modelling 38 (2012) 226–234

Contents lists available at SciVerse ScienceDirect

Journal of Molecular Graphics and Modelling

journal homepage: www.elsevier.com/locate/JMGM

Coupled motions during dynamics reveal a tunnel toward the active site regulated by the N-terminal α-helix in an acylaminoacyl peptidase

Elena Papaleo*,[1], Giulia Renzetti[1]

Department of Biotechnology and Biosciences, University of Milano-Bicocca, P.zza della Scienza 2, 20126 Milan, Italy

ARTICLE INFO

Article history:
Accepted 26 June 2012
Available online 7 July 2012

Keywords:
Acylaminoacyl peptidase
Molecular dynamics simulations
Prolyl oligopeptidase
Correlated motions
Extremophilic enzyme
Conformational changes

ABSTRACT

Acylaminoacyl peptidase (AAP) subfamily belongs to the prolyl oligopeptidase (POP) family of serine-proteases. There is a great interest in the definition of molecular mechanisms related to the activity and substrate recognition of these complex multi-domain enzymes. The active site relies at the interface between the C-terminal catalytic domain and the β-propeller domain, whose N-terminal region acts as a bridge to the hydrolase domain. In AAP, the N-terminal extension is characterized by a structurally conserved α1-helix, which is known to affect thermal stability and thermal dependence of the catalytic activity. In the present contribution, results from hundreds nanosecond all-atom molecular dynamics simulations, along with analyses of the networks of cross-correlated motions of a member of the AAP subfamily are discussed. The MD investigation identifies a tunnel that from the surrounding of the N-terminal α1-helix bring to the catalytic site. This cavity seems to be regulated by conformational changes of the α1-helix itself during the dynamics. The evidence here provided can be a useful guide for a better understanding of the mechanistic aspects related to AAP activity, but also for drug design purposes.

1. Introduction

It is nowadays well accepted that protein dynamics is strictly related to protein function [1–4], as well as that the conformational transitions to functionally competent states can be intrinsically accessible by fluctuations around the protein native state [5,6]. The description of enzymes, in a dynamics framework is therefore strongly encouraged and can provide remarkable insights both for the comprehension of the underlying molecular mechanisms and also for the design and development of active molecules.

Atomistic molecular dynamics (MD) simulations turned out a suitable tool to investigate conformational changes and protein dynamics signatures around the protein native state [4,7,8], in particular considering the notion that a direct link between the different timescales in protein dynamics exists. In fact, the observation of dynamics on shorter ps or ns timescales can provide information on events likely to happen on higher timescales, if the suitable techniques to decode this information are available [1,9]. For example, the analysis of the cross-correlations of the atomic fluctuations [10–13] provided useful hints on protein dynamics and even allosteric effects [12,14–17]. In general, residues that feature patterns of clearly correlated motions are associated with protein thermal stability and functional dynamics [12,18,19]. Moreover, it has been suggested that critical residues associated either with protein function or with the maintenance of the three-dimensional (3D) architecture can co-evolve [20,21].

In this context, we focus our attention on dynamical cross-correlated motions of the acylaminoacyl peptidase (AAP) subfamily, which belong to the prolyl oligopeptidase (POP) family [22]. AAP catalyzes the removal of an N-acylated amino acid from different blocked peptides [23,24]. Only the X-ray structure of one member of the AAP subfamily; the acylaminoacyl peptidase from *Aeropyrum pernix* K1 (ApAAP, E.C. 3.4.19.1) [25] is available in the Protein Data Bank. Indeed, the investigation of structural and mechanistic aspects related to AAP function is of crucial importance since AAPs are appealing both for industrial purposes [26–31] and as pharmacology targets [22,32,33]. In fact, deficiency in human AAP has been correlated to cancer diseases [34] and AAP inhibition is known to favor apoptosis [35]. AAP is also a potential site for cognition-enhancing drugs [36].

ApAAP is a homodimeric enzyme, in which each subunit is characterized by two domains; a N-terminal β-propeller domain (residue 1–324) and a C-terminal catalytic α/β hydrolase domain (residues 325–581) (Fig. 1A) [25]. The catalytic triad is located in the C-terminal hydrolase domain (Ser445, Asp524 and His556). Particular attention was also dedicated to the N-terminal α-helix (α1, residues 8–21 in ApAAP, pdb entry 1VE6 [37]), which is a common motif of the prolyl oligopeptidase (POP) family [22]. α1-Helix connects the N- and the C-terminal domain and it is not conserved in terms of primary sequence and secondary structure along the POP family [37]. In fact, it was demonstrated that the

* Corresponding author.
E-mail address: elena.papaleo@unimib.it (E. Papaleo).
[1] The authors equally contributed to this work.

1093-3263/$ – see front matter © 2012 Elsevier Inc. All rights reserved.
http://dx.doi.org/10.1016/j.jmgm.2012.06.014

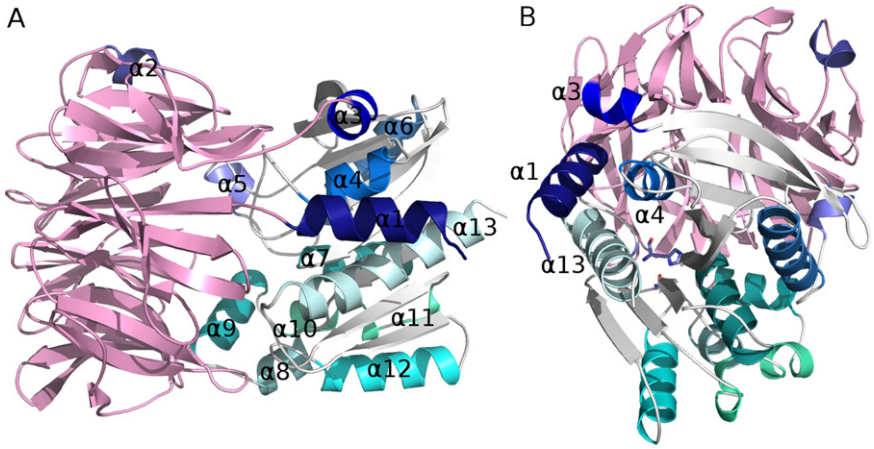

Fig. 1. ApAAP 3D structure. (A) Overall 3D structure of wild-type ApAAP (pdb entry 1VE6), with the N-terminal β-propeller domain colored in pink and the C-terminal catalytic domain colored in white. The α-helices are shown in different shade of blues from N- to C-terminal extremity. (B) Side view of the 3D structure of wild-type ApAAP in the region at the interface between C-terminal and N-terminal extremity with highlighted α1, α3, α4 and α13. The catalytic triad is shown as sticks. (For interpretation of the references to color in this figure legend, the reader is referred to the web version of the article.)

deletion of the whole N-terminal α1-helix (deletion of residues 1–21, Δ21-ApAAP) affects temperature-dependence of ApAAP activity [37]. Neverthless, the 3D structure of the Δ21-ApAAP was experimentally solved (pdb entry 2QZP) and it did not show relevant modifications in the overall 3D structure and in its dimerization properties [28]. Several mechanisms have been proposed for the substrate recognition or the product release both in AAP and in the whole POP family, relying on conformational changes of different enzyme regions [22,38,39]. In particular, it has been recently shown that AAP [40] is likely to be characterized by the same mechanism for substrate recognition proposed for other POP members [41–44] in which the opening of the interface between the two domains is required for the access of the substrate to the catalytic site. However, the underlying details can change, with AAP for example characterized by a conformational selection mechanism in which open and closed states could co-exist in solution [40].

In light of the above observation, this contribution showed results from hundreds nanoseconds all-atom molecular dynamics (MD) simulations of wild-type ApAAP with particular attention to cavity detection and networks of coupled motions during dynamics in the proximity of the N-terminal α1-helix, which acts as a bridge between the two AAP domains. It turns out a high flexibility of the N-terminal α1-helix with few local cross-correlated motions. Moreover, a "tunnel", which brings to the catalytic site and is regulated by conformational changes of the α-helix itself and its surroundings, is evident in the MD ensemble.

2. Materials and methods

2.1. α-Helices definition

The secondary structures were assigned according to DSSP [45] and α-helices numbered according to the definition provided in ref. [25] for ApAAP. It includes 13 α-helices numbered as: α1 (10–21), α2 (239–243), α3 (324–329), α4 (380–387), α5 (405–409), α6 (418–432), α7 (446–457), α8 (474–480), α9 (483–493), α10 (497–502), α11 (505–511), α12 (529–541) and α13 (561–579). α1 and α2 belong to the β-propeller domain, whereas from α3 to α13 to the catalytic domain.

2.2. Molecular dynamics (MD) simulations

The X-ray structure of AAP from *Aeropyrum pernix* K1 (ApAAP, pdb entry 1VE6 [25]), along with wild-type ApAAP in an open conformation (pdb entry 3O4G [40]) and a truncated mutant of ApAAP carrying the deletion of the N-terminal α1-helix (ApAAP-Δ21, pdb entry 2QZP [28]) were used as initial structures for the MD simulations by GROMACS 3.3.3 software package (www.gromacs.org)

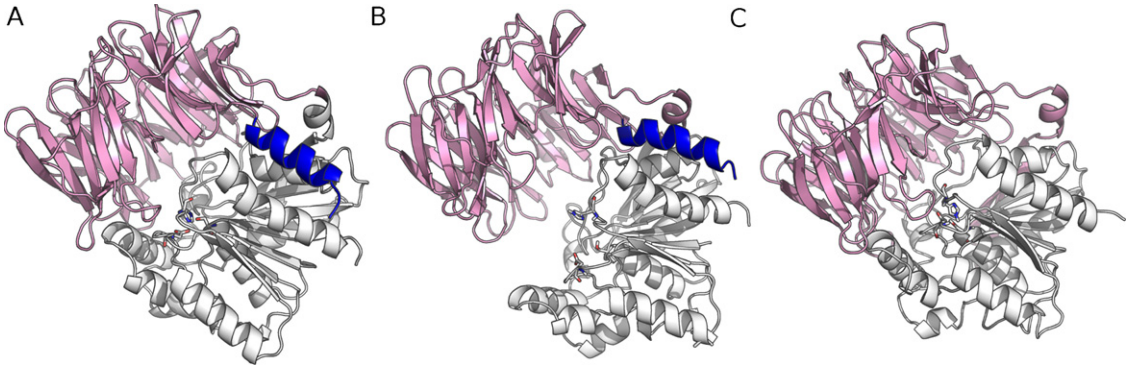

Fig. 2. Starting structures for the MD simulations. The 3D X-ray structures of ApAAP used as starting structures for the MD simulations; wild-type ApAAP in closed (pdb entry 1VE6, panel A) and open conformation (pdb entry 3O4G, panel B), as well as a variant carrying a deletion of α1-helix ApAAP-Δ21 (pdb entry 2QZP, panel C). The N-terminal β-propeller domain is colored in pink, whereas the C-terminal catalytic domain is colored in white and the N-terminal α1-helix in blue. The catalytic triad is shown as sticks. (For interpretation of the references to color in this figure legend, the reader is referred to the web version of the article.)

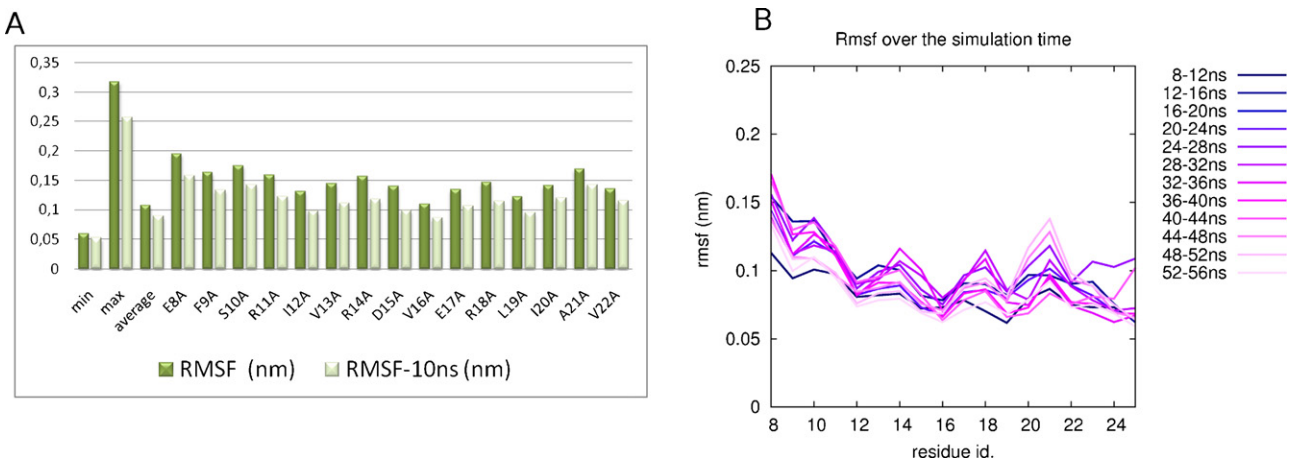

Fig. 3. Flexibility of α1-helix. (A) Average values of per-residue Cα rmsf of residues belonging to α1-helix and its immediate surroundings, compared to average, minimum and maximum rmsf values for the whole protein. Rmsf profiles were calculated both as per-residue averages of the rmsf values from each independent MD trajectories, as well as per-residue averages of rmsf values calculated along time-windows of 10 ns. (B) Time evolution of Cα rmsf profiles of α1 residues and its immediate surroundings calculated as rmsf profiles over non-overlapping 4 ns time-windows. For sake of clarity only the example referred to MD replica 1 of wild-type ApAAP is reported.

implemented on a parallel architecture, using GROMOS96 43a1 force field.

The starting structures were soaked in a dodecahedral box of SPC (simple point charge) water molecules [46] using periodic boundary conditions, with a minimum distance between the solute and the box of 0.7 nm. In order to neutralize the overall charge of the system, a number of water molecules equal to the protein net charge were replaced by Na^+ ions.

The system was initially relaxed by molecular mechanics (steepest descent, 10,000 steps), the optimization step was followed by 50 ps of solvent equilibration at 283 K (time step 1 fs and thermal coupling constant of 1 fs), while restraining the protein atomic positions using an harmonical potential. The system was slowly driven to the target temperature (300 K) and pressure (1 bar) through a thermalization and a series of pressurization simulations of 50 ps each. The same preparation procedure was carried out for ApAAP in an open conformation and ApAAP-Δ21, as well as for a short control MD simulation of the wt dimeric ApAAP (4 ns).

Productive 50/100 ns MD simulations were carried out in the isothermal-isobaric (NPT) ensemble, using the Berendsen thermostat with a coupling constant of 0.1 ps at 300 K. Pressure was kept constant (1 bar) by modifying the box dimensions and the time-constant for pressure coupling was set to 1 ps. The LINCS algorithm [47] was used to constrain heavy atoms bond lengths, allowing the use of a 2 fs time-step. Long-range electrostatic interactions were calculated using Particle-Mesh Ewald (PME) summation scheme [48]. Van der Waals and Coulomb interactions were truncated at 1.0 nm. The non-pair list was updated every 10 steps and conformations were stored every 4 ps. To identify recurring features and to avoid simulations artifacts two independent simulations (replicas) were carried out for the full-length ApAAP.

2.3. Analysis of MD simulations

The main chain root mean square deviation (rmsd), which is a crucial parameter to evaluate the stability of MD trajectories, was computed using as a reference the starting structure of the MD simulations. The first 5 ns of each simulations were discarded to ensure stability of the trajectories. To carefully check the stability of the rmsd profiles, sample simulations were extended to 100 ns in order to verify that the resulting trajectories were consistently stable.

The analysis of the secondary structure (ss) content was carried out using the DSSP program [45], along with the calculation of the most frequently attained secondary structure for each residue was evaluated to obtain a residue-dependent persistence degree of secondary structure profile to check stability of the secondary structure elements (*data not shown*).

Correlation plots were obtained by computing Cα dynamical cross-correlation matrices (DCCM) $C(i,j)$ [11], using non over-lapping averaging windows of 1 ns, and also compared, for validation, to correlations on averaging windows of 5 and 10 ns. $C(i,j)$ was calculated according to,

$$C(i,j) = \frac{c(i,j)}{c(i,i)^{1/2}c(j,j)^{1/2}}$$

where $c(i,j)$ is the element of the covariance matrix of protein fluctuations between residues i and j.

Only the most significant ($|C(i,j)| > 0.4$) long range ($|i-j| > 12$) positive and negative correlations were considered. The cutoff of sequence distance was selected in order to exclude from the analysis correlations relative to the inner α-helix structures and contiguous in the primary sequence. Moreover, since we discuss an average $C(i,j)$ matrix, a cutoff of 0.4 (in absolute value) for significant correlations was selected to exclude from the analyses pairs of residues, which are poorly communicating each other and

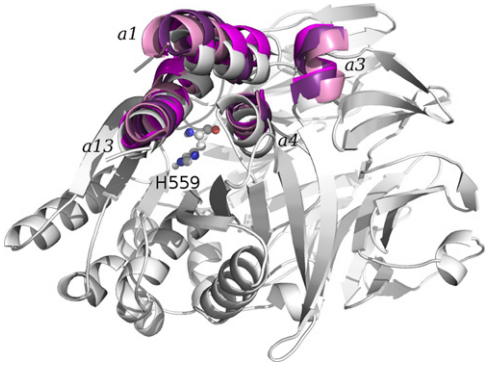

Fig. 4. Snapshots from the MD simulations. Representative snapshots from the MD trajectories of wild-type ApAAP have been superimposed and the conformations of helices α1, α3, α4 and α13 are highlighted with different shade of colors form white (first steps of the simulations) to purple (final frames of the simulations) in each snapshot. (For interpretation of the references to color in this figure legend, the reader is referred to the web version of the article.)

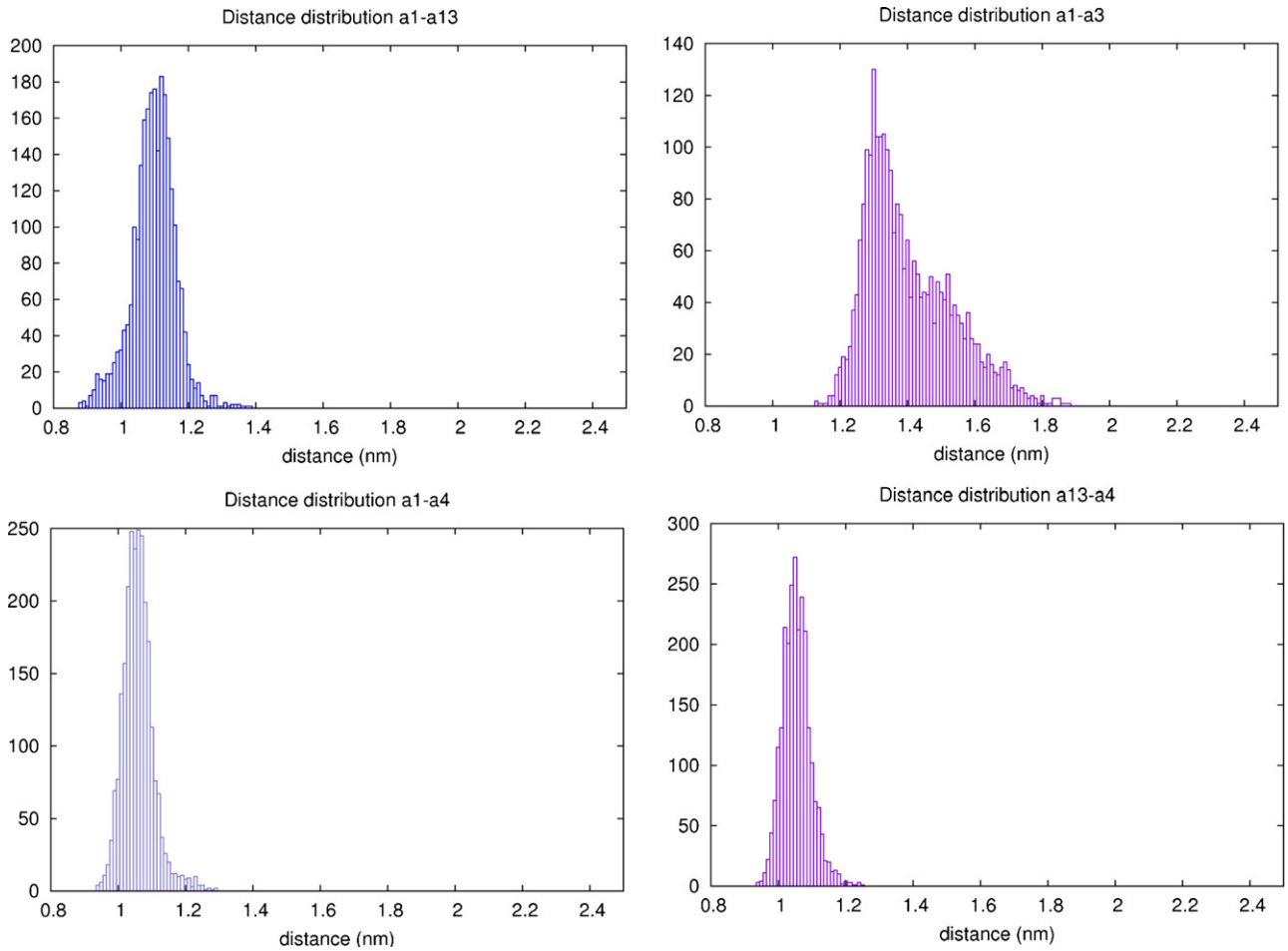

Fig. 5. Distance distributions between α-helices in the surrounding of the interface between N- and C-terminal extremities. The distributions of distances between the center of mass of α1 and α3, α4 and α13, respectively are shown, along with the distribution of distances between the center of mass of α4 and α13.

likely to be characterized by uncoupled motions. To verify that the analysis of an average $C(i,j)$ matrix does not cause a loss of relevant information, the consistency between the average $C(i,j)$ matrix with the individual matrices used in the averaging was also evaluated. To assess the sensitivity of the selected cutoff of correlation intensity, average $C(i,j)$ matrices were also analyzed filtering the matrix at lower (0.30 and 0.35) or higher cutoffs (0.45 and 0.5).

To provide a description along the simulation time of the correlated motions, the DCCM time-evolution was analyzed, employing non-overlapping DCCM calculated over 1, 2.5 or 5 ns time-windows. Correlations were then plotted on the 3D structure by connecting atoms i and j by lines, of thickness proportional to $C(i,j)$.

The per-residue Cα root mean square fluctuation (rmsf) was calculated with respect to the average structure. To properly assess the consistency of the flexibility profile, per-residue rmsf were computed both on the whole trajectories, and also as average rmsf profiles calculated on 10 and 4 ns time-windows.

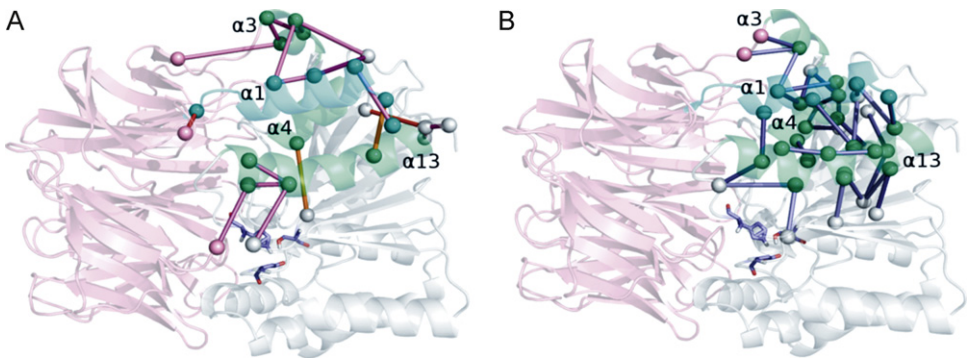

Fig. 6. Salt bridge, aromatic and hydrophobic interactions. (A) The salt bridge and aromatic pairs are indicated by lines, colored from deep-purple to pink and from red to yellow, respectively. The residues involved in the interactions and their networks are shown as spheres. (B) The hydrophobic interactions are indicated by lines colored from density blue to light-blue and the residues involved are represented as spheres. The α-helices and the two protein domains are colored according to Fig. 1.

The distances between the α1 helix and α3, α4, α13 helices were monitored during the simulations by the Gromacs tool g_dist that calculates the distances between the two groups involved in the interaction.

The salt bridge interactions were evaluated as oppositely charged groups at less than 0.45 nm of distance in at least 20% of the macro-trajectory frames. For aromatic (and amino-aromatic) and hydrophobic interactions, a distance cutoff of 0.6 and 0.5 nm was employed. Also the angles between the groups involved in the electrostatic interactions were carefully checked before collecting the results. The persistence cutoff of 20% was selected as the persistence value which best divided the interaction dataset in well-separated groups, defines as signal and noise, according to a protocol previously applied [49]. Moreover, to verify the consistency of our analyses, the salt bridges were also computed employing both 0.4 and 0.5 nm of distance cutoffs and lower persistence cutoff (*data not shown*). To well identify on the 3D structure networks of salt bridge, hydrophobic or aromatic interactions, for each class, the residues involved in the interactions were represented as nodes of an unrooted unoriented graph, in which two nodes were connected by arcs if a salt bridge was identified between them.

CAST-p (Computed Atlas of Surface Topography of proteins) [50] was employed to identify pockets and cavities of the protein during dynamics, with particular attention to the interface between the C- and N-terminal extremity, using snapshots from the MD simulations collected each 50 ps. The analysis with CAST-p was also carried out on the dimeric structure of the enzyme to validate the formulated hypotheses.

Table 1
Salt bridge, aromatic and hydrophobic interactions that involves residues belonging to helices α1, α3, α4, α13 during the simulations.

Residues pairs	Persistence%	Residues pairs	Persistence%
Eletrostatic interactions			
ASP553:LYS566	47.23	VAL572:ALA388	49.49
GLU562:LYS566	52.44	LEU575:PHE390	52.26
LYS85:ASP563	50.74	ALA571:VAL466	57.39
ASP563:LYS566	43.52	ALA387:LEU19	49.1
ARG18:ASP325	24.39	ALA383:ILE330	81.53
ARG18:ASP325	24.39	ALA576:ILE12	23.86
ASP325:ARG328	35.8	ALA383:LEU19	95.77
GLU324:ARG328	44.02	ALA564:ILE558	71.42
GLU319:ARG327	23.04	ILE567:ILE558	22.92
GLU324:ARG327	43.46	VAL392:ALA382	95.05
ASP15:ARG18	35.53	ALA564:ILE20	79.12
ASP15:ARG355	95.61	LEU326:LEU322	30.02
ASP325:ARG355	42.35	PHE574:ALA517	99.98
GLU8:ARG11	38.26	ALA386:ILE330	90.32
GLU438:ARG579	38.91	LEU575:VAL466	41
ARG579:GLU580	55.3	ALA571:ILE519	53.51
Aromatic interactions			
TYR444:PHE381	53.15	ALA576:PHE9	66.52
PHE573:PHE9	41.53	LEU326:LEU19	27.45
ARG579:PHE390	79.87	PHE573:LEU569	31.46
PHE41:LYS24	91.61	LEU569:VAL565	42.73
Hydrophobic interactions			
ALA382:LEU351	22.39	ALA388:ILE12	82.07
PRO570:ILE519	27.83	ILE567:PRO521	23.96
ALA386:LEU351	66.38	PHE574:VAL466	27.01
VAL572:VAL16	65.86	VAL392:ALA386	22.79
LEU568:PHE381	48.43	LEU326:PRO323	67.36

3. Results and discussion

In the present contribution, all-atom explicit solvent MD simulations were carried out at 300 K for the wild-type ApAAP, in its closed and open conformations (Fig. 2A and B), and for a variants which brings a deletion of α1 residues (ApAAP-Δ21, Fig. 2C). Particular attention was devoted to the interface region between the N-terminal α1-helix and the surrounding α-helices in the catalytic C-terminal domain. A minor role in protein dimerization was pointed out for α1-helix [28], in agreement with few interactions mediated by the helix at the dimeric interface and high B-factor values in the crystallographic dimeric form [25]. Moreover, the conformation of one monomer within the ApAAP dimer is independent of the conformation of the other, so that the two monomers were suggested to act independently [40]. In light of these observations, we primarily decided to focus our attention on the dynamic properties of the monomeric form and then to verify our results also on the dimeric variant.

3.1. N-Terminal α1-helix is a flexible structural element acting as a bridge between C-terminal α-helices of the catalytic domain

The N-terminal α1-helix acts as a bridge between the β-propeller domain and the catalytic domain (Fig. 1B) and it is therefore an element of particular interest to monitor during dynamics. In particular, it turns out from our simulations that α1-helix is characterized by a high flexibility in terms of root mean square fluctuation (rmsf), both on the whole MD timescale and as average rmsf employing 10 ns time-windows (Fig. 3A). Remarkably, each residue of the helix features rmsf values higher than the rmsf average values calculated for the whole protein (Fig. 3A).

To further investigate dynamics properties of the N-terminal α1-helix, the rmsf profiles were also followed along the simulations

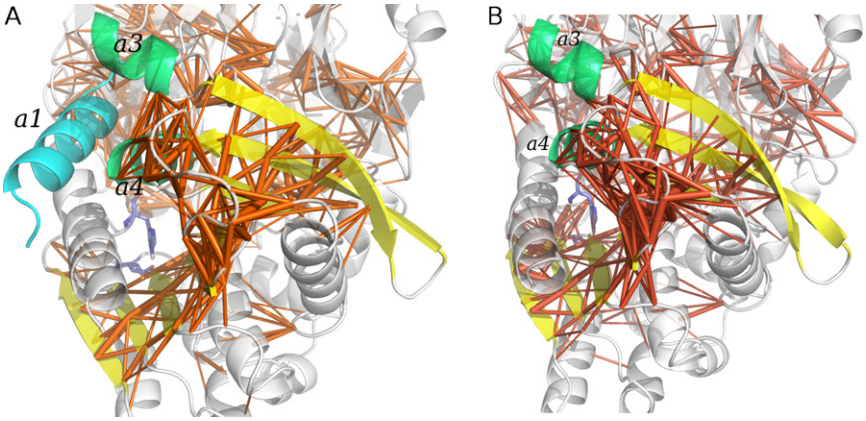

Fig. 7. The tunnel toward the catalytic site formed by α1 and the β-sheet of the catalytic domain in wt ApAAP (A) and modification in ApAAP-Δ21 (B). The catalytic residues are indicated as sticks. Cross-correlation between residues, calculated from a 5 ns average DCCM and a cutoff for significant correlation of 0.45, are indicated as tick lines connecting each pair of correlated residues.

time, collecting rmsf profiles calculated on non-overlapping time-windows of 2 ns each (Fig. 3B). It turns out an oscillatory tendency of α1-helix flexibility, which alternatively tends to increase and decrease along the simulation time.

3.2. During dynamics, α1, α4 and α13-helices oscillates between different conformational states

In the 3D structure, α1 is located at the interface between C-terminal α13 and α4 helices. In their proximity also α3 maps, placed almost perpendicular with respect to both α1 and α4 (Fig. 1B). The visual inspection of the simulation frames indicates that the modification in α1 flexibility, at different simulation times, correlates with different orientation of the α1-helix with respect to the aforementioned surrounding helices. In fact, α1-helix can populate both states in which it approaches the α13 and α4 faces, as well as conformations in which α1 features an outward displacement (Fig. 4). On the contrary, the spatial positions of α13 and α3 are not particularly affected by the α1-helix movements, whereas α4 shows the most relevant effects and features dynamical behavior comparable to α1-helix. To better assess these effects, the reciprocal distances between the center of mass of α1 and the surrounding helices were monitored during the simulation time, along with the distance between α13 and α4. In agreement with the visual inspection of the simulations, the distance between α1 and α4 is the most stable during the simulations time, along with the distance between α4 and α13, whereas the other distances show higher fluctuations and variability (Fig. 5). Interestingly, the α1 flexibility profiles and its conformational changes are a common feature of all the ApAAP trajectories (Fig. 2A), pointing out an intrinsic characteristic of the ApAAP native state.

3.3. α1-Helix is necessary to provide the correct spatial disposition of the surrounding helices

In this context, the α1 high flexibility and its capability to populate different conformations in the native state, can suggest a low propensity of the helix to form stable and high persistence interactions during the MD simulations. Therefore, a network representation, previously applied to salt bridge interactions [49,51] was here employed to identify the intramolecular interactions and their networks mediated by α1, α3, α4 and α13 in terms of salt bridges, aromatic and hydrophobic interactions (Fig. 6). It turns out, in agreement with the scenario so far described, that few interactions are located in these regions and most of them mediated by α1 residues (Table 1). In particular, most of the interactions are characterized by a low or average persistence indicating weak interactions that during protein dynamics can break and reform and only few interactions have a high persistence in almost all the snapshots. Among the latter, there are the salt bridge between D15 and R355, also previously experimentally investigated [37] and the amino-aromatic interaction between F41 and K24 located at the end of the α1 region.

To better assess the contribution of α1 to the spatial disposition of the surrounding helices, ApAAP-Δ21 simulations were analyzed. In particular, in ApAAP-Δ21, in absence of α1-helix, a reciprocal rearrangement can be observed for α13 (in gray) and α4, approaching each other (Fig. 7B), and therefore perturbing the network of intramolecular interactions and communication nearby. The emerging scenario from our MD investigations is that α1-helix is required to allow the proper orientation of several residues in the C-terminal regions, in particular in α13, α4 and α3 helices.

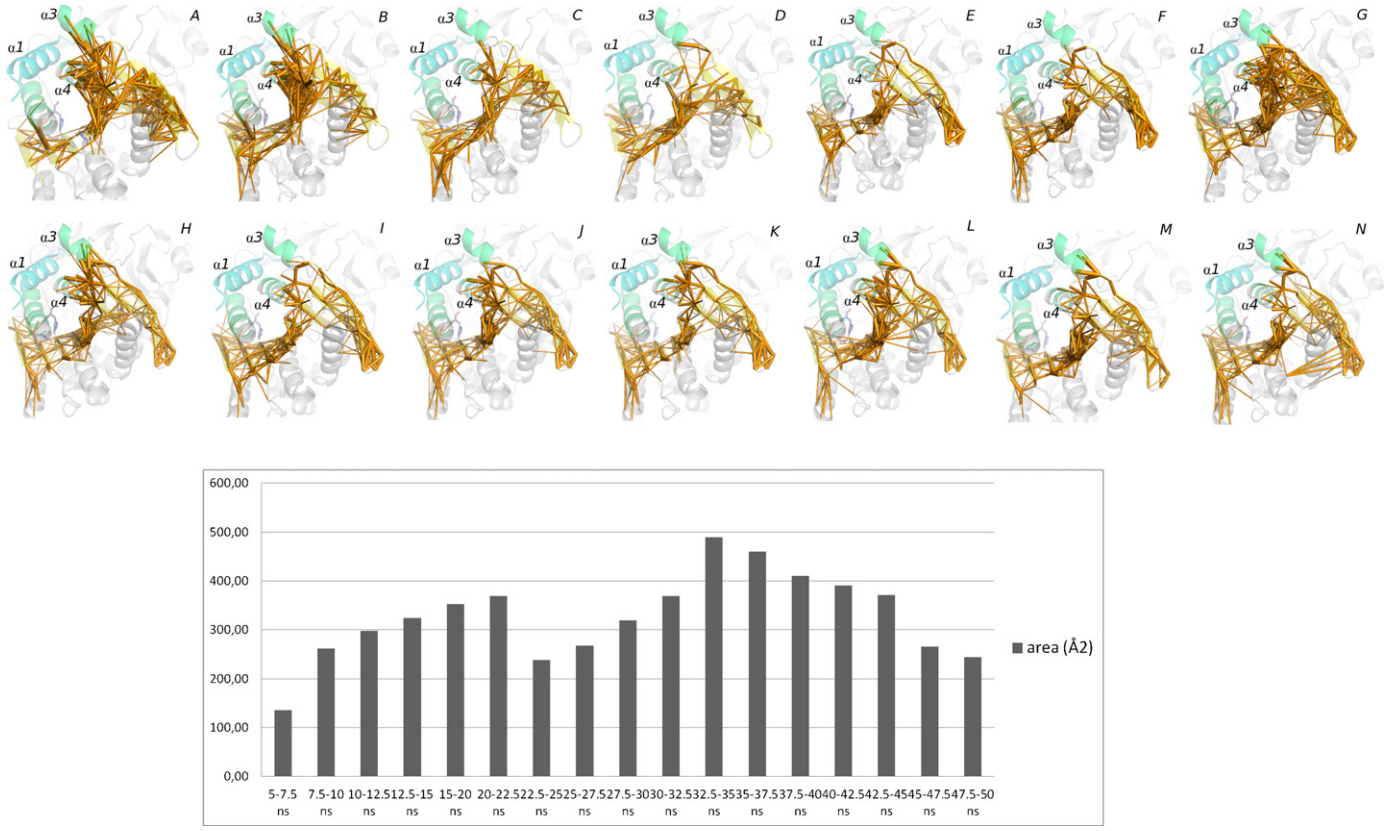

Fig. 8. Evolution of network of correlated residues in the proximity of the tunnel (A) and size of the cavity (B). (A) The catalytic residues are indicated as sticks. Cross-correlation between residues calculated every 2.5 ns and a cutoff for significant correlation of 0.45 are indicated as tick lines connecting each pair of correlated residues. (B) The average size of the cavity modulated by α1-helix conformational changes for each 2.5 ns time-window in the 50 ns simulation.

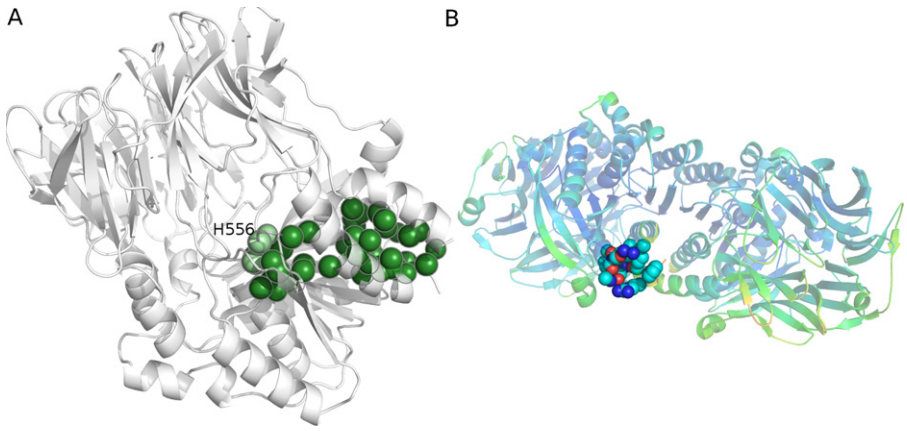

Fig. 9. The tunnel structure toward the catalytic site. The residues in the "dynamics" pocket which from the α1-helix and its surrounding directly bring to the catalytic site and include the catalytic hystidine are represented by the green spheres and have been calculated by CASTp [50] in both the monomeric (A) and dimeric form (B). (For interpretation of the references to color in this figure legend, the reader is referred to the web version of the article.)

The networks of coupled residues during dynamics allow to define a tunnel-like structure toward the catalytic site.

The data collected so far from MD analyses prompted us to further investigate protein dynamics of ApAAP in the surrounding of the interface between the C- and N-terminal elements. In fact, the visual inspection of the MD conformational ensemble points out not only the outward movement of α1, which also approaches the external side of the C-terminal α13 (Fig. 4), but also an opening of a "tunnel" bringing to the active site, which has not been identified yet in AAP or POP-like proteins, as far as we know. In fact, to characterized in details this aspect, we evaluate the distribution on the 3D structure of the network of coupled residues derived by the analysis of dynamical cross-correlation matrices (DCCM, see Section 2). The most significant coupled motions on different timescales (1–5–10 ns) were calculated and plotted on a reference 3D structure. Different correlation cutoffs of 0.4, 0.45 and 0.5 (in absolute value) were tested to evaluate the most relevant pairs of positively and negatively correlated residues and to filter out poorly and not significant coupled residues. In particular, on the considered timescales and correlation cutoffs, only positively coupled residues were identified in the C-terminal regions where the aforementioned helices reside. Interestingly, the helices α1 and α13 do not feature, over the different time-windows, a great number of correlated motions with other protein regions, on the contrary their dynamics is generally decoupled from those of the rest of the protein (Figs. 7A and 8 upper panels).

Instead, the ApAAP β-sheet of the catalytic domain feature a tight network of cross-correlations which maintained the reciprocal arrangement of the β-strands forming the β-sheet itself (Figs. 7A and 8 upper panels). α1 and α13 helices are therefore provided by a sufficient degree of flexibility to modulate the access to the catalytic site and their motions decoupled from the rest of the protein structure, whereas the C-terminal β-sheet and its internal coupled motions provide a stable "floor" for this cavity, and coupled motions mediated by helices α3 and α4 allow a rigid structure which can close one site of the cavity (Figs. 7 and 8 upper panels). In fact, α4 (residues 378–388) features a tight networks of coupled motions during the simulations between element internal to the catalytic domain itself, but also with residues at the extremity of the β-propeller domain (Figs. 7 and 8 upper panels), concurring to the intermolecular interface between the two domains.

The detection of the cavity is also confirmed by analyses with CASTp [50]. The 50 ns simulation was divided in 2.5 ns time windows and the average size of the cavity was calculated for each of them (Fig. 8 lower panel). In the snapshots with α-1 featuring the outward displacement, a pocket of approximately 350–450 Å^2 was identified. This cavity directly bring from the regions where the bundle of helices is located to the active site and also includes, among the pocket residues, the catalytic His556 (Fig. 9A). The analysis of the dimeric ApAAP structure in a dynamics framework (4 ns) also features, according to CASTp analysis, the presence of a cavity in the corresponding region (Fig. 9B) (average area of 341 Å^2), enforcing the conclusion here provided by the analysis of the monomer dynamics.

4. Conclusions

In the present contribution, hundreds nanosecond all-atom MD simulations of a representative member of the AAP subfamily (*Aeropyrum pernix* K1) allow to identify the presence of a tunnel which from the surrounding of the N-terminal α1-helix bring to the catalytic site and it is regulated by conformational changes of the N-terminal α1-helix itself and its surroundings in the native conformational ensemble. This dynamics cavity is a common and inherent feature of both ApAAP closed and open (competent for substrate binding) states, which are likely to coexist in the native conformational ensemble of the protein [40].

The emerging picture from our dynamic investigation here presented is that α1-helix is required to allow the correct orientation of several residues in the C-terminal regions, in particular in α13, α3 and α4 helices. These residues, in turns, provide both the reciprocal stabilization of the interdomain interfaces and a proper architecture of the catalytic site. However, none of the residues of α1 alone could account for this effect, since they can compensate each other and have a highly variable nature during the dynamics. In fact, α1 helix is characterized at the same time by the sufficient number and persistence of intramolecular interactions to maintain part of the interface between the two protein domains and to long-range communicate with the active site, but also it is provided by a sufficient degree of flexibility and local uncoupled motions. This inherent flexibility allow the interconversion between conformational states in which is at the interface between α13 and α4 and other states in which, thanks to an outward movement, it can open a tunnel toward the catalytic site.

Recently, several mechanisms were proposed for the access of the substrate to the catalytic site across the cavity in the β-propeller, identified in the ApAAP X-ray structure [25] and by electron microscopy of a POP enzyme [43]. Moreover, recently it has been proposed, by the study of D524 mutant variants and ApAAP wild-type protein, that an equilibrium can exist between ApAAP open and closed conformations, in which a cavity for the substrate access can be formed at the interface between the β-propeller

blades and the catalytic domain [40]. To complicate the scenario, very recently the possible binding pathways of an inhibitor of the porcine POP enzyme were explored by both steered molecular dynamics (SMD) and umbrella sampling (US), suggesting an exit pathway through the beta-propeller tunnel and a flexible loop at the inter-domain interface [52]. Further studies will be therefore necessary to provide a complete understanding of mechanisms involved in substrate recognition and release in the AAP subfamily, but even in a broader context for the POP members. In fact, efforts were dedicated to the study, by different simulation techniques, of the binding and release of inhibitor molecules to other POP enzymes [52,53], attesting the interest in these directions, but still poor details are available for the AAP members.

The evidences here provided are likely to be an useful guide both for a better understanding of the mechanistic aspects related to AAP activity, but also, even more interestingly, for drug design purposes. In fact, our results can stimulate future investigations aimed to assess if there is any biological relevance for the cavity here identified, which is still to clarify. In fact, it might provide access of small substrates or release of the products, but further studies are necessary. The fluctuations of AAP α1-helix in the native conformational ensemble, along with its intrinsic property to populate states providing an access to the catalytic site points out a potential site that can be appealing for docking studies or design of active molecules.

Acknowledgements

We thank Luca De Gioia and Gaetano Invernizzi for careful reading of the manuscript and their suggestions. This research was supported by CASPUR (Consorzio Interuniversitario per le Applicazioni di Supercalcolo per Università e Ricerca) Standard HPC Grant 2010 and 2011 to E.P.

References

[1] J. Villali, D. Kern, Choreographing an enzyme's dance, Current Opinion in Chemical Biology 14 (2010) 636–643.
[2] P. Csermely, R. Palotai, R. Nussinov, Induced fit, conformational selection and independent dynamic segments: an extended view of binding events, Trends in Biochemical Sciences 35 (2010) 539–546.
[3] V.C. Nashine, S. Hammes-Schiffer, S.J. Benkovic, Coupled motions in enzyme catalysis, Current Opinion in Chemical Biology 14 (2010) 644–651.
[4] M. Rueda, C. Ferrer-Costa, T. Meyer, A. Perez, J. Camps, A. Hospital, J.L. Gelpi, M.M. Orozco, A consensus view of protein dynamics, Proceedings of the National Academy of Sciences of the United States of America 104 (2007) 796–801.
[5] I. Bahar, C. Chennubhotla, D. Tobi, Intrinsic dynamics of enzymes in the unbound state and, relation to allosteric regulation, Current Opinion in Structural Biology 17 (2007) 633–640.
[6] S.R. Tzeng, C.G. Kalodimos, Protein dynamics and allostery: an NMR view, Current Opinion in Structural Biology 21 (2011) 62–67.
[7] G.G. Dodson, D.P. Lane, C.S. Verma, Molecular simulations of protein dynamics: new windows on mechanisms in biology, EMBO Reports 9 (2008) 144–150.
[8] P.I. Zhuravlev, C.K. Materese, G.A. Papoian, Deconstructing the native state: energy landscapes, function, and dynamics of globular proteins, Journal of Physical Chemistry B 113 (2009) 8800–8812.
[9] K.A. Henzler-Wildman, M. Lei, V. Thai, S.J. Kerns, M. Karplus, D. Kern, A hierarchy of timescales in protein dynamics is linked to enzyme catalysis, Nature 450 (2007) 913–927.
[10] R.A. Estabrook, J. Luo, M.M. Purdy, V. Sharma, P. Weakliem, T.C. Bruice, N.O. Reich, Statistical co evolution analysis and molecular dynamics: identification of amino acid pairs essential for catalysis, Proceedings of the National Academy of Sciences of the United States of America 102 (2005) 994–999.
[11] P.H. Hunenberger, A.E. Mark, W.F. Van, Gunsteren, Fluctuation and cross-corelation analysis of protein motions observed in nanosecond molecular dynamics simulations, Journal of Molecular Biology 252 (1995) 492–503.
[12] D. Armenta-Medina, E. Perez-Rueda, L. Segovia, Identification of functional motions in the adenylate kinase (ADK) protein family by computational hybrid approaches, Proteins 79 (2011) 1662–1671.
[13] B.L. Kormos, A.M. Baranger, D.L. Beveridge, A study of collective atomic fluctuations and cooperativity in the U1A-RNA complex based on molecular dynamics simulations, Journal of Structural Biology 157 (2007) 500–513.
[14] M. Tozluoglu, E. Karaca, R. Nussinov, T. Halilogiu, A mechanistic view of the role of E3 in sumoylation, PLoS Computational Biology (2010) 6.
[15] F.F.F. Schmid, M. Meuwly, All-atom simulations of structures and energetics of c-di-GMP-bound and free PleD, Journal of Molecular Biology 374 (2007) 1270–1285.
[16] L. Li, V.N. Uversky, A.K. Dunker, S.O. Meroueh, A computational investigation of allostery in the catabolite activator protein, Journal of the American Chemical Society 129 (2007) 15668–15676.
[17] S. Cheng, M.Y. Niv, Molecular dynamics simulations and elastic network analysis of protein kinase B (Akt/PKB) inactivation, Journal of Chemical Information and Modeling 50 (2010) 1602–1610.
[18] K.L. Mayer, M.R. Earley, S. Gupta, K. Pichumani, L. Regan, M.J. Stone, Covariation of backbone motion throughout a small protein domain, Natural Structural Biology 10 (2003) 962–965.
[19] E. Rhoades, E. Gussakovsky, G. Haran, Watching proteins fold one molecule at a time, Proceedings of the National Academy of Sciences of the United States of America 100 (2003) 3197–3202.
[20] S.W. Lockless, R. Ranganathan, Evolutionarily conserved pathways of energetic connectivity in protein families, Science 286 (1999) 295–299.
[21] G.M. Suel, S.W. Lockless, M.A. Wall, R. Ranganathan, Evolutionarily conserved networks of residues mediate allosteric communication in proteins, Natural Structural Biology 10 (2003) 232.
[22] R. Van Elzen, A.M. Lambeir, Structure and function relationship in prolyl oligopeptidase, CNS Neurol Disord Drug Targets 10 (2011) 297–305.
[23] S. Tsunasawa, K. Narita, K. Ogata, Purification and properties of acylamino-acid-releasing enzyme from rat-liver, Journal of Biochemistry 77 (1975) 89–102.
[24] C.W. Sokolik, T.C. Liang, F. Wold, Studies on the specificity of actelylaminoacyl-peptide hydrolase, Protein Science 3 (1994) 126–131.
[25] M. Bartlam, G.G. Wang, H.T. Yang, R.J. Gao, X.D. Zhao, G.Q. Xie, S.G. Cao, Y. Feng, Z.H. Rao, Crystal structure of an acylpeptide hydrolase/esterase from *Aeropyrum pernix* K1, Structure 12 (2004) 1481–1488.
[26] A.L. Kiss, B. Hornung, K. Radi, Z. Gengeliczki, B. Sztaray, T. Juhasz, Z. Szeltner, V. Harmat, L. Polgar, The acylaminoacyl peptidase from *Aeropyrum pernix* K1 thought to be an exopeptidase displays endopeptidase activity, Journal of Molecular Biology 368 (2007) 509–520.
[27] Z. Szeltner, A.L. Kiss, K. Domokos, V. Harmat, G. Naray-Szabo, L. Polgar, Characterization of a novel acylaminoacyl peptidase with hexameric structure and endopeptidase activity, Biochimica et Biophysica Acta – Proteins & Proteomics 1794 (2009) 1024–1210.
[28] H.F. Zhang, B.S. Zheng, Y. Peng, Z.Y. Lou, Y. Feng, Z.H. Rao, Expression, purification and crystal structure of a truncated acylpeptide hydrolase from *Aeropyrum pernix* K1, Acta Biochimica et Biophysica Sinica 37 (2005) 613–617.
[29] E.A. Brunialti, P. Gatti-Lafranconi, M. Lotti, Promiscuity, stability and cold adaptation of a newly isolated acylaminoacyl peptidase, Biochimie 93 (2011) 1543–1554.
[30] Q.Y. Wang, G.Y. Yang, Y.L. Liu, Y. Feng, Discrimination of esterase and peptidase activities of acylaminoacyl peptidase from hyperthermophilic *Aeropyrum pernix* K1 by a single mutation, Journal of Biological Chemistry 281 (2006) 18618–18625.
[31] C. Liu, G. Yang, L. Wu, G. Tian, Z. Zhang, Y. Feng, Switch of substrate specificity of hyperthermophilic acylaminoacyl peptidase by combination of protein and solvent engineering, Protein & Cell 2 (2011) 497–506.
[32] P. Morain, P. Lestage, G. De Nanteuil, R. Jochemsen, J.L. Robin, D. Guez, P.A. Boyer, S 17092: a prolyl endopeptidase inhibitor as a potential therapeutic drug for memory impairment. Preclinical and clinical studies, CNS Drug Reviews 8 (2002) 31–52.
[33] K. Toide, K. Okamiya, Y. Iwamoto, T. Kato, Effect of a novel prolyl endopeptidase inhibitor, JTP-4819, on prolyl endopeptidase activity and substance-p-like and arginine–vasopressin-like immunoractivity in the brains of aged rats, Journal of Neurochemistry 65 (1995) 234–240.
[34] R. Erlandsson, F. Boldog, B. Persson, E.R. Zabarovsky, R.L. Allikmets, J. Sumegi, G. Klein, H. Jornvall, The gene from the short arm of chromosome-3, at D3F15S2, frequently deleted in renal-cell carcinoma, encodes acylpeptide hydrolase, Oncogene 6 (1991) 1293–1295.
[35] M. Yamaguchi, D. Kambayashi, J. Toda, T. Sano, S. Toyoshima, H. Hojo, Acetylleucine chloromethyl ketone, an inhibitor of acylpeptide hydrolase, induces apoptosis of U937 cells, Biochemical and Biophysical Research Communications 263 (1999) 139–142.
[36] P.G. Richards, M.K. Johnson, D.E.D.E. Ray, Identification of acylpeptide hydrolase as a sensitive site for reaction with organophosphorus compounds and a potential target for cognitive enhancing drugs, Molecular Pharmacology 58 (2000) 577–583.
[37] Z.M. Zhang, B.S. Zheng, Y.P. Wang, Y.Q. Chen, G. Manco, Y. Feng, The conserved N-terminal helix of acylpeptide hydrolase from archaeon *Aeropyrum pernix* K1 is important for its hyperthermophilic activity, Biochimica et Biophysica Acta – Proteins & Proteomics 1784 (2008) 1176–1183.
[38] Z. Szeltner, L. Polgar, Structure, function and biological relevance of prolyl oligopeptidase, Current Protein and Peptide Science 9 (2008) 96–107.
[39] V. Fulop, Z. Bocskei, L. Polgar, Prolyl oligopeptidase: an unusual beta-propeller domain regulates proteolysis, Cell 94 (1998) 161–170.
[40] V. Harmat, K. Domokos, D.K. Menyhard, A. Pallo, Z. Szeltner, I. Szamosi, T. Beke-Somfai, G. Naray-Szabo, L. Polgar, Structure and catalysis of acylaminoacyl peptidase closed and open subunits of a dimer oligopeptidase, Journal of Biological Chemistry 286 (2011) 1987–1998.
[41] M. Fuxreiter, C. Magyar, T. Juhasz, Z. Szeltner, L. Polgar, I. Simon, Flexibility of prolyl oligopeptidase: molecular dynamics and molecular framework analysis of the potential substrate pathways, Proteins 60 (2005) 504–512.

[42] L. Shan, I.I. Mathews, C. Khosla, Structural and mechanistic analysis of two prolyl endopeptidases: role of interdomain dynamics in catalysis and specificity, Proceedings of the National Academy of Sciences of the United States of America 102 (2005) 3599–3604.
[43] T. Tarrago, J. Martin-Benito, E. Sabido, B. Claasen, S. Madurga, M. Gairi, J.M. Valpuesta, E. Giralt, A new side opening on prolyl oligopeptidase revealed by electron microscopy, FEBS Letters 583 (2009) 3344–3348.
[44] M. Li, C. Chen, D.R. Davies, T.K. Chiu, Induced-fit mechanism for prolyl endopeptidase, Journal of Biological Chemistry 285 (2010) 21487–21495.
[45] W. Kabsch, C. Sander, Dictionary of protein secondary structure: pattern recognition of hydrogen-bonded and geometrical features, Biopolymers 22 (1983) 2577–2637.
[46] M. Fuhrmans, B.P. Sanders, S.J. Marrink, A.H. de Vries, Effects of bundling on the properties of the SPC water model, Theoretical Chemistry Accounts 125 (2010) 335–344.
[47] B. Hess, H. Bekker, H.J.C. Berendsen, J. Fraaije, LINCS: a linear constraint solver for molecular simulations, Journal of Computational Chemistry 18 (1997) 1463–1472.
[48] T. Darden, D. York, L. Pedersen, Particle mesh Ewald – an nlog(n) method for Ewald sums in large systems, Journal of Chemical Physics 98 (1993) 10089–10092.
[49] M. Tiberti, E. Papaleo, Dynamic properties of extremophilic subtilisin-like serine-proteases, Journal of Structural Biology 174 (2011) 69–83.
[50] J. Dundas, Z. Ouyang, J. Tseng, A. Binkowski, Y. Turpaz, J. Liang, CASTp: computed atlas of surface topography of proteins with structural and topographical mapping of functionally annotated residues, Nucleic Acids Research 34 (2006) W116–W118.
[51] E. Papaleo, M. Pasi, M. Tiberti, L. De Gioia, Molecular dynamics of mesophilic-like mutants of a cold-adapted enzyme: insights into distal effects induced by the mutatations, PLoS One 6 (2011) e24214.
[52] J.F. St-Pierre, M. Karttunen, N. Mousseau, T. Rog, A. Bunker, Use of umbrella sampling to calculate the entrance/exit pathway for Z-Pro-prolinal inhibitor in prolyl oligopeptidase, Journal of Chemical Theory and Computation 7 (2011) 1583–1594.
[53] K. Kaszuba, T. Rog, J.F. St Pierre, P.T. Mannisto, M. Karttunen, A. Bunker, Molecular dynamics study of prolyl oligopeptidase with inhibitor in binding cavity, SAR and QSAR in Environmental Research 20 (2009) 595–609.